AD-A090 637 VIRGINIA UNIV CHARLOTTESVILLE DEPT OF MATERIALS SCIENCE F/G 11/6
DUCTILE FRACTURE INITIATION IN PURE ALPHA-FE,(U)
AUG 80 R N GARDNER, H G WILSDORF N00014-75-C-0691
UNCLASSIFIED UVA/525354/MS80/101 NL

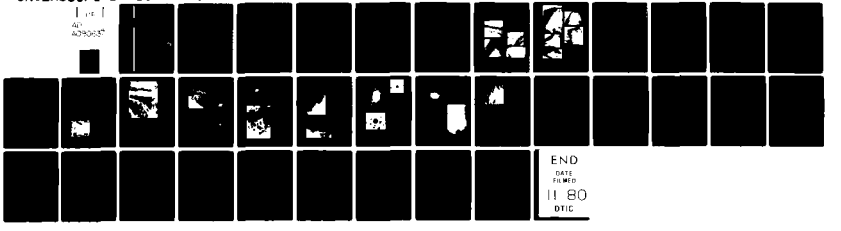

RESEARCH LABORATORIES FOR THE ENGINEERING SCIENCES

SCHOOL OF ENGINEERING AND APPLIED SCIENCE

UNIVERSITY OF VIRGINIA

Charlottesville, Virginia 22901

A Report

DUCTILE FRACTURE INITIATION IN PURE α-Fe

Submitted to:

Office of Naval Research
800 N. Quincy Street
Arlington, Virginia 22217

Submitted by:

R. N. Gardner

H. G. F. Wilsdorf
Professor

Contract N00014-75-C-0691

Report No. UVA/525354/MS80/101

August 1980

RESEARCH LABORATORIES FOR THE ENGINEERING SCIENCES

Members of the faculty who teach at the undergraduate and graduate levels and a number of professional engineers and scientists whose primary activity is research generate and conduct the investigations that make up the school's research program. The School of Engineering and Applied Science of the University of Virginia believes that research goes hand in hand with teaching. Early in the development of its graduate training program, the School recognized that men and women engaged in research should be as free as possible of the administrative duties involved in sponsored research. In 1959, therefore, the Research Laboratories for the Engineering Sciences (RLES) was established and assigned the administrative responsibility for such research within the School.

The director of RLES—himself a faculty member and researcher—maintains familiarity with the support requirements of the research under way. He is aided by an Academic Advisory Committee made up of a faculty representative from each academic department of the School. This Committee serves to inform RLES of the needs and perspectives of the research program.

In addition to administrative support, RLES is charged with providing certain technical assistance. Because it is not practical for each department to become self-sufficient in all phases of the supporting technology essential to present-day research, RLES makes services available through the following support groups: Machine Shop, Instrumentation, Facilities Services, Publications (including photographic facilities), and Computer Terminal Maintenance.

A Report

DUCTILE FRACTURE INITIATION IN PURE α-Fe

Submitted to:

Office of Naval Research
800 N. Quincy Street
Arlington, Virginia 22217

Submitted by:

R. N. Gardner

H. G. F. Wilsdorf
~~Professor~~

(15) N00014-75-C-0641

Department of Materials Science
RESEARCH LABORATORIES FOR THE ENGINEERING SCIENCES
SCHOOL OF ENGINEERING AND APPLIED SCIENCE
UNIVERSITY OF VIRGINIA
CHARLOTTESVILLE, VIRGINIA

(12) 15

Report No. UVA/525354/MS80/101

Aug~~ust~~ 1980

Copy No. 1

401 162

ABSTRACT

Single crystal α-Fe whiskers, grown by the reduction of ferrous chloride by hydrogen have been strained to fracture in an Instron tensile testing machine and in a bench straining device at various elongation rates at room temperature. Whiskers were found to exhibit macroscopic slip behavior strongly dependent upon elongation rate while the geometric reduction in area and the fracture mode remained in all cases identical. Ductile rupture of iron whiskers produces a characteristically shaped chisel-edge fracture whose geometry is sensitive to crystal orientation, due to the geometry of active slip systems, but which is not a function of strain rate. The micromechanisms of ductile rupture of these single crystals are strongly affected by dislocation dynamics. The development of dislocations necessary to accommodate an extensive reduction in area appears to be independent of the nature of surface slip observed. Dislocation structures form small volume elements which are separated from one another by dislocation cell walls. The accommodation of large strains as well as the reduction in area is determined by the movement of dislocations on the order of a distance equal to that of the dislocation cell size. The boundaries of the cell and/or the cell volume could then be expected to be specifically related to the site where the initiation of fracture occurs.

α-Fe single crystals of high purity were strained to fracture by in-situ high voltage electron microscopy. This method permitted recording of events leading to the failure of the crystal at high magnifications. Specifically, observations were made regarding the first step in the fracture mechanism, namely the initiation of voids, which occurred after a dislocation pattern of cells had developed. The cell size was found to be a few tens of nanometers in diameter and, because of the small scale of the dislocation patterns, a direct observation of void initiation was not possible. However, the misorientation between cells could be determined by electron diffraction techniques leading to the conclusion that void initiation took place at cell walls and at the boundaries of deformation microtwins. The high energy of these interfaces is another factor supporting the above conclusion.

Ductile Fracture Initiation in Pure α-Fe: Part I. Macroscopic Observations of the Deformation History and Failure of Crystals

R. N. GARDNER AND H. G. F. WILSDORF

Reprinted from

METALLURGICAL TRANSACTIONS A
VOLUME 11A, NUMBER 4

Physical Metallurgy and Materials Science
APRIL 1980

Ductile Fracture Initiation in Pure α-Fe: Part I. Macroscopic Observations of the Deformation History and Failure of Crystals

R. N. GARDNER AND H. G. F. WILSDORF

Single crystal α-Fe whiskers, grown by the reduction of ferrous chloride by hydrogen have been strained to fracture in an Instron tensile testing machine and in a bench straining device at various elongation rates at room temperature. Whiskers were found to exhibit macroscopic slip behavior strongly dependent upon elongation rate while the geometric reduction in area and the fracture mode remained in all cases identical. Ductile rupture of iron whiskers produces a characteristically shaped chisel-edge fracture whose geometry is sensitive to crystal orientation, due to the geometry of active slip systems, but which is *not* a function of strain rate. The micromechanisms of ductile rupture of these single crystals are strongly affected by dislocation dynamics. The development of dislocations necessary to accomodate an extensive reduction in area appears to be independent of the nature of surface slip observed. Dislocation structures form small volume elements which are separated from one another by dislocation cell walls. The accommodation of large strains as well as the reduction in area is determined by the movement of dislocations on the order of a distance equal to that of the dislocation cell size. The boundaries of the cell and/or the cell volume could then be expected to be specifically related to the site where the initiation of fracture occurs.

THE mode of ductile fracture in metals and alloys is dependent upon the dislocation structures that evolve during the deformation history of a crystal. The failure of a single crystal as a result of simple shear on a primary glide plane is well understood whereas rupture of a similar crystal necessitates a more complex arrangement of dislocations and requires a detailed description of phenomena occurring during necking. From this description we may then identify those sites where the initiation of fracture will occur.

The basic concepts involved in fracture initiation in clean metals have been derived from a number of macroscopic observations of the strain rate dependence of the appearance of glide on the surface of metal crystals, the observed geometry of reduction in area of α-Fe single crystals, as well as a complete description of the deformation history of single crystal iron whiskers strained to fracture.[1,2] Verification of the implied micromechanisms of fracture has been insured by their direct observation during *in situ* straining in the High Voltage Electron microscope.[3-6] The dependence of slip trace depth on elongation rate in conjunction with the observation that the geometric reduction in area is elongation rate independent demands an accounting of dislocation movements on the order of a small volume rather than the large distances giving rise to slip steps. This is of fundamental importance to a description of the micromechanisms of fracture. The information gained as a result of this study has helped to elucidate several critical features of ductile fracture of metals in general.

R. N. GARDNER is Senior Research Scientist, 3M Company, 3M Center, Central Research Laboratories, St. Paul, MN 55101, and H. G. F. WILSDORF is Wills Johnson Professor of Materials Science, School of Engineering and Applied Science, University of Virginia, Charlottesville, VA 22901.

Manuscript submitted October 16, 1978.

EXPERIMENTAL

Crystals were grown by the reduction of ferrous chloride by hydrogen. The exact nature of crystal growth and geometries of crystals obtained from the growth processes have been summarized elsewhere.[7] Crystals whose initial gage length approximated in all cases 0.5 cm, were strained to fracture in an Instron tensile testing machine as well as a bench straining device, at elongation rates varying from 10^{-7} cm/s to 8.33×10^{-2} cm/s. Crystals were characterized both before and after deformation in the scanning electron microscope (SEM) and through the use of the X-ray precession method.[8]

All crystals in this study were taken from the same batch (growth boat) in order to minimize effects of uncontrolled variation in quality and composition.

RESULTS

High purity single crystal α-Fe whiskers with their stress axes parallel to ⟨110⟩, ⟨111⟩, ⟨211⟩, or ⟨100⟩ were strained to fracture. The strengths of these crystals varied systematically with orientation and were found to be in the range of 0.6 to 9×10^8 pascals (Pa).

Three-stage hardening was uniformly exhibited by the majority of crystals studied, as was almost 100 pct reduction in area, *i.e.*, chisel edge fracture. The chisel edge fracture appeared 'crystallographic' in nature. That is, edges of certain orientations were consistently along identical directions, these directions being related to the initial geometry, and reductions in area repeatedly demonstrated the same geometric behavior as will be summarized later.

The subsequent geometries of crystals strained at two different elongation rates i) 7×10^{-7} cm/s, and ii) 8.33×10^{-5} cm/s, are compared in the micrographs shown in Fig. 1(*a*) and (*b*) and demonstrate the depend-

ISSN 0360-2133/80/0411-0653$00.75/0

ence of surface slip trace depth on elongation rate. However, the formation of either planar or wavy slip depends upon the number of active slip systems. The more numerous the active slip systems, the wavier is the appearance of slip. The formation of coarse wavy slip (Fig. 2(*a*)) was observed in crystals that were elongated at the slowest rate, 10^{-7} cm/s, used in this study. What is consistent throughout the slow elongation rate experiments is the coarseness of the slip traces, and, where few slip systems are active, slip packet formation.

The crystal shown in Fig. 1(*a*) has been observed by "shadow" contrast, *i.e.*, the contrast obtained from the outline of a nontransmissionable crystal under the electron beam in the HVEM at an elongation rate of about 7×10^{-6} cm/s. Glide packets were observed to have formed by abrupt slip, *i.e.*, the formation of a large slipped area in an abrupt or jerky motion. The large slip packets seen may be due to some type of channel formation[9] or slip instability.[10]

Crystals strained in an Instron tensile testing machine at an elongation rate of 8.33×10^{-4} cm/s still exhibited coarse slip, yet little packet formation was observed. Where small slip packets formed, small yield points occurred along the length of the three-stage hardening curves.

Finally, at the higher elongation rates tested, it became increasingly difficult to image discrete traces in the SEM due to inadequate resolution (200A). At the highest elongation rates at which specimens were strained, that is at 8.33×10^{-2} cm/s, the appearance of glide on the surface of crystals was in the form of very fine traces. These results vary only slightly with crystal orientation and such differences, again, depend only upon the number of slip systems activated.

Each crystal of a particular crystallographic orientation demonstrated the same geometry of the reduced area of the fractured end regardless of the rate at which it was strained to failure. Figure 3 shows this geometry in three crystals strained at three elongation rates, while the overall geometry is that shown in

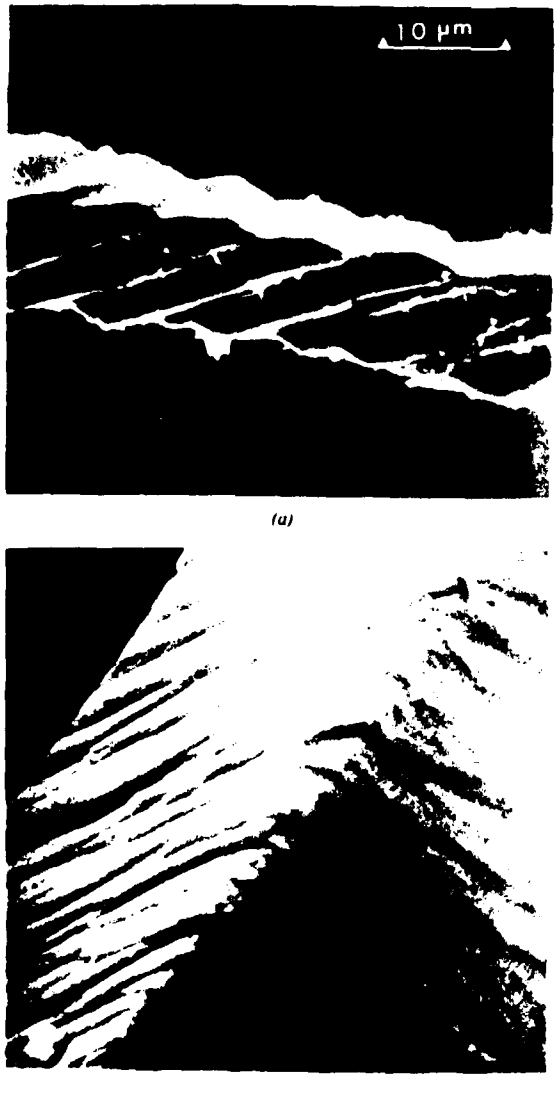

(*a*)

(*b*)

Fig. 1—SEM micrographs of crystals oriented with tensile axis parallel to <100>. The appearance of glide on the surface has been found to differ with elongation rate in that decreasing coarseness and depth of slip (decreasing distance between slip steps) results from increasing strain rate. (See also Figs. 2 thru 4). The crystals are viewed from the side. These crystals, whose initial gage length approximated, in all cases, 0.8 cm, have been strained at (*a*) 7×10^{-7} cm/s, and (*b*) 8.33×10^{-4} cm/s.

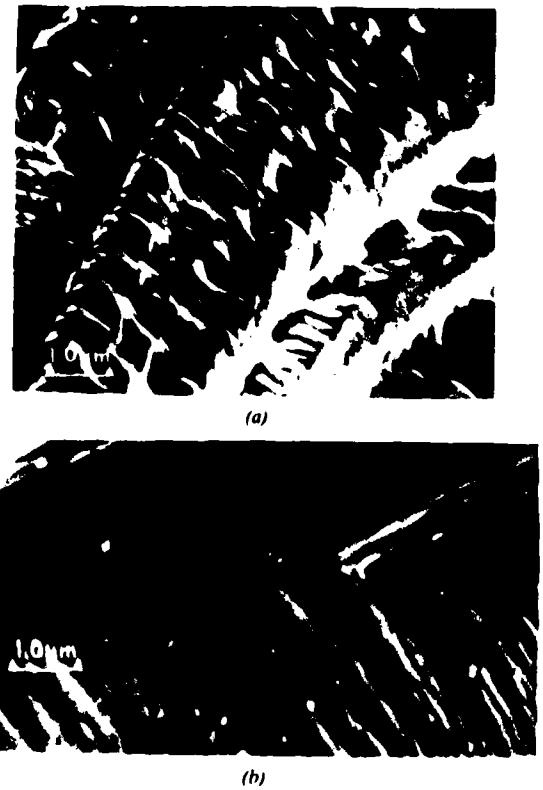

(*a*)

(*b*)

Fig. 2—SEM micrograph of crystals oriented in tension along the <110> direction. Again the appearance of glide on the surface has been found to vary with elongation rate. SEM resolution estimated at 200 Å was not able to resolve slip line structure on crystals strained at elongation rates higher than 10^{-3} cm/s. These crystals have been subject to a constant elongation rate of (*a*) 6×10^{-7} cm/s, and (*b*) 8.33×10^{-4} cm/s. The crystals' fracture tips are viewed from the side.

(a)

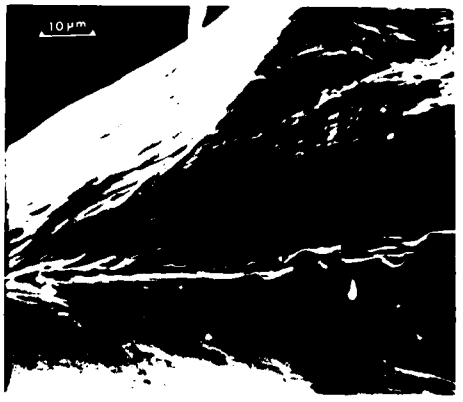

(b)

(c)

Fig. 3 SEM micrograph of three crystals having tensile axes oriented along the <110> direction that have been strained at elongation rates of (*a*) 6×10^{-7} cm/s, (*b*) 8.33×10^{-5} cm/s, and (*c*) 8.33×10^{-2} cm/s. The resultant crystallography of reduction in area is independent of elongation rate. The fracture tips of crystals are viewed "end-on".

Figs. 5(*a*), 3, and 4 (representing crystals whose tensile axes are oriented along the ⟨110⟩ and ⟨100⟩ respectively) demonstrate that the mode of fracture in these whiskers is independent of elongation rate.

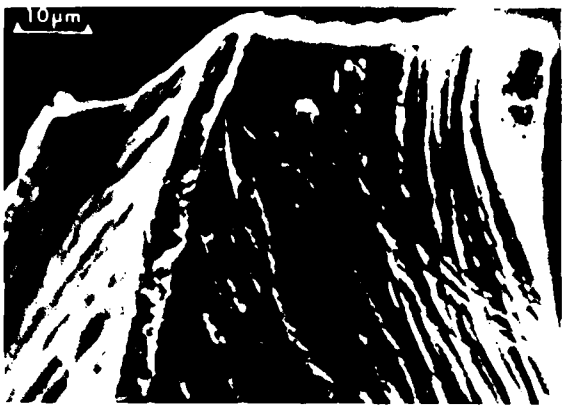

(a)

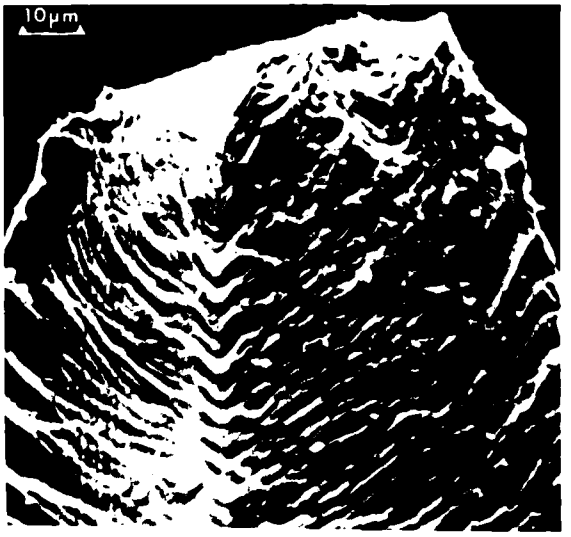

(b)

Fig. 4 SEM micrograph of crystals having a <100> tensile axis, display similar failure geometries, but exhibit slightly differing slip behavior. The elongation rates were (*a*) 5×10^{-6} cm/s, and (*b*) 8.33×10^{-5} cm/s. The fracture tips of crystals are viewed from the sides of the ends.

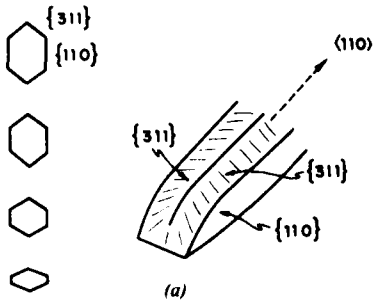

(a)

Fig. 5 Summary of the reduction in area and cross-sectional changes of α-Fe whiskers. In all cases, the uniform development of a chisel edge is seen.

A summary of cross-sectional changes of the whiskers preceding chisel edge fracture is given in Fig. 5. The development of the chisel edge is quite uniform specifically, there is invariably an invariant direction along which there is no reduction in length, while that direction which is perpendicular to both the aforementioned invariant direction and the longitudinal axis of the crystal exhibits a 100 pct reduction in length.[1]

The findings of the precession method indicate that i) large lattice rotations are continuous and are at a maximum about the invariant axis, and ii) rotations of volume elements are discovered to be both clockwise and counterclockwise about the invariant axis.[8] These results are consistent with the determination of the dependence of slip trace depth on elongation rate.

While the slip trace depth was dependent upon both elongation rate and the movement of dislocations over large distances, the same fracture behavior was observed in crystals subjected to higher elongation rates and all samples of similar orientation exhibited comparable amounts of volume rotation.

The geometry of reduction in area is dependent upon volume rotations about an invariant axis. This axis is a ⟨110⟩ crystallographic direction. As seen in Fig. 6, this would be expected from the activation of ⟨111⟩ slip directions. Crystals only experience reduction in length along crystallographic directions or axes which are perpendicular to those axes about which maximum volume

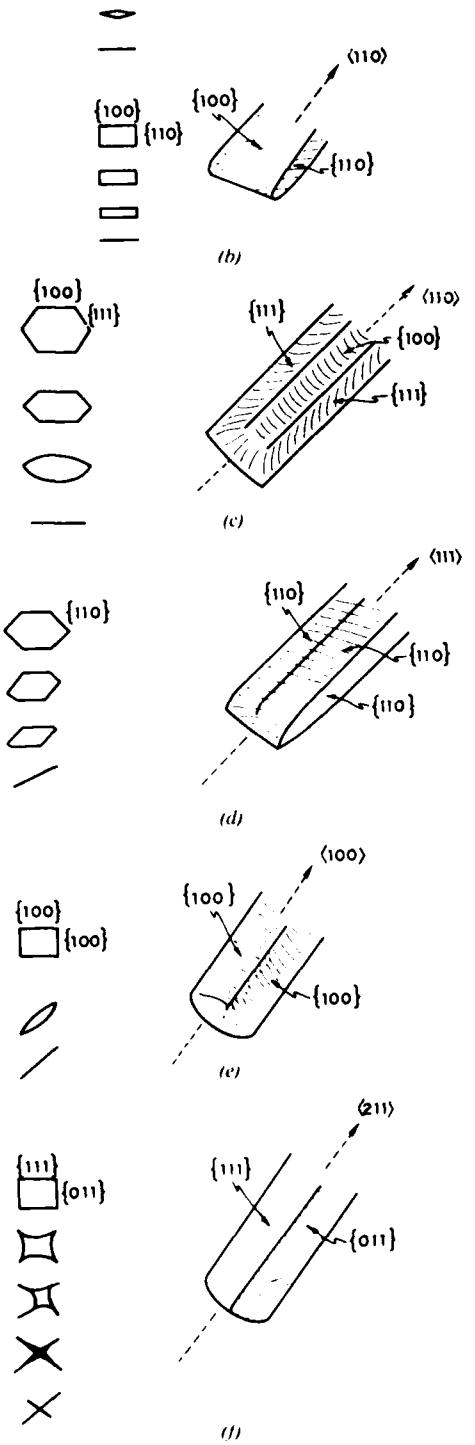

Fig. 5—Continued.

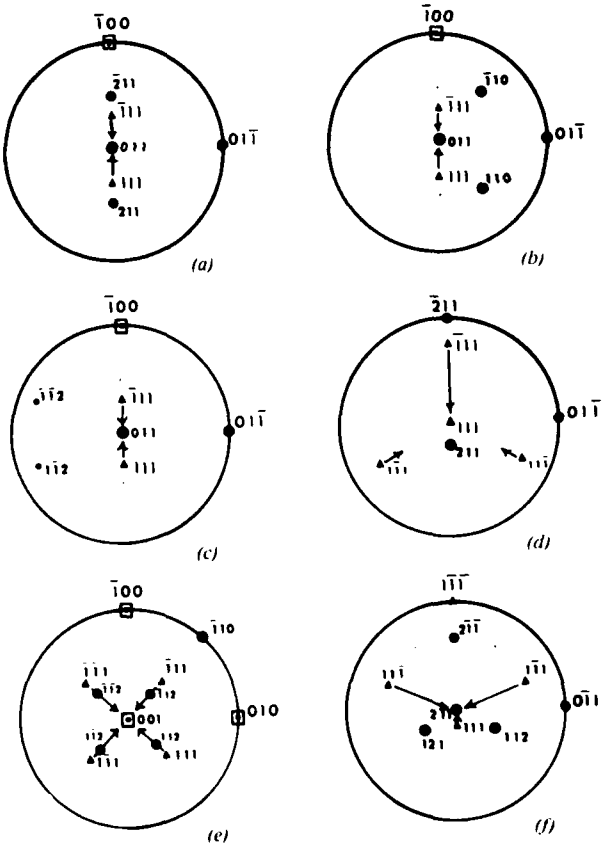

Fig. 6—Summary of Burgers vectors, active during the necking process, that give rise to the experimentally observed geometries of reduction in area of Fig. 5(*a*) thru (*f*). Large lattice rotations invariably are seen to take place about an ⟨011⟩ axis. One might expect, since these rotations are due to rotating volume elements, that when the degree of rotation is so large as to align the original active slip direction with the tensile axis, the appearance of a polycrystalline texture would result. Hence, it would not be unusual to obtain ⟨110⟩ texture diffraction patterns from the crack flank of all of these crystals.

Table I. Summary of Active Glide Systems Leading to Fracture

External Geometry	Tensile Axis	Primary Active Slip System in the Neck of Crystals
A	[011]	$(\bar{2}11)[111], (211)[\bar{1}11]$
glide off*	[011]	$(\bar{1}10)[111]$
B	[011]	$(\bar{1}10)[111], (101)[\bar{1}11]$
C	[011]	$(\bar{1}\bar{1}2)[111], (12\bar{1})[\bar{1}11]$
glide off*	[111]	$(211)[\bar{1}11]$
D	[111]	$(211)[\bar{1}11], (112)[11\bar{1}], (121)[1\bar{1}1]$
glide off*	[001]	$(\bar{1}\bar{2}3)[111]$ $(\bar{1}\bar{1}2)[111]$ $(\bar{2}\bar{1}3)[111]$
E	[001]	$(\bar{1}\bar{1}2)[111], (112)[\bar{1}\bar{1}1]$ $(\bar{1}12)[1\bar{1}1], (1\bar{1}2)[\bar{1}11]$
F	[211]	$(2\bar{1}\bar{1})[111], (112)[11\bar{1}], (121)[1\bar{1}1]$

*If simple glide off were to occur, the active slip system which would be responsible is given.

Table II. Some Initial Schmid Factors of Pertinent Slip Systems*

Tensile Direction	Slip System	Initial Schmid Factor
[011]	$(211)[\bar{1}11]$	0.47
	$(\bar{3}12)[111]$	0.46
	$(101)[\bar{1}11]$	0.41
[111]	$(211)[\bar{1}11]$	0.31
	$(312)[\bar{1}11]$	0.30
	$(110)[\bar{1}11]$	0.27
	$(12\bar{1})[\bar{1}11]$	0.15
[001]	$(1\bar{1}2)[\bar{1}11]$	0.47
	$(\bar{1}\bar{2}3)[111]$	0.46
	$(011)[1\bar{1}1]$	0.41
[211]	$(100)[11\bar{1}]$	0.41
	$(112)[11\bar{1}]$	0.39
	$(2\bar{1}1)[111]$	0.31
	$(\bar{3}12)[111]$	0.30

*A complete listing of Schmid factors has been compiled previously.[1]

rotation does take place. While over 100 crystals were strained to fracture, this was consistently found to be the case. Table I summarizes the active glide systems and designates those systems which may give rise to simple glide off and Table II gives the relevant Schmid factors. The active slip systems were determined by slip trace analysis. Shear fracture was only observed to occur twice.

DISCUSSION

The correlation between the macroscopically observed slip lines and the dislocation arrangements causing these surface steps is complex. For extremely slow elongation rates of 10^{-7} cm/s where atypical structures are observed, one expects in bcc metals that the mode of deformation itself differs from that mode controlling the deformation processes at higher elongation rates.[11] That is, one may assume that the mechanism overcoming the Peierls friction for dislocation motion is not rate-controlling and that the mobility of screw dislocations at extremely slow rates of strain is governed by the non-conservative motion of jogs.[11]

It is assumed, then, that dislocation dynamics dictate a consistent determining mechanism for dislocation motion over the range of elongation rates from 10^{-6} to 10^{-2} cm/s.[12,13] However, the rate of uniform cell development is expected to vary with strain as well as with strain rate. During increasing strain, cell development will become complete and cells will shrink in size by the process of similitude.[14,15] Deformed crystals in which dislocations have some degree of three-dimensional mobility and where there are several mutually independent noncoplanar slip systems contain dislocation configurations which approach that of ideal minimum energy storage. When a crystal experiences an increasing strain rate, cell size shrinks rapidly and the lowest energy configuration is unattainable as a result.

The relative magnitudes of stored energy of these networks can be expected to vary with loop size.[16] As one would expect, the larger the loops, the smaller the energy per unit area. Hence, it is observed that crystals experiencing slow strain rates will have larger three-dimensional cell networks than those crystals experiencing high strain rates.

Microscopically, only those segments of dislocations which shear cells are visible, although it is, of course, recognized that dislocation continuity is required The passage of dislocations through large networks, then, will give rise to discretely spaced slip steps. The passage of large numbers of dislocations over the considerable distance represented by the crystal may cause the appearance of slip packets as well as the appearance of 'slip channels'. Hence, it is probable that with decreasing cell size, the appearance of glide on the surface of the crystal becomes finer and finer.

Of particular importance is the observation that the geometry of the reduction in area which results from straining these whiskers is independent of the strain rate. The precession method indicates that large lattice rotations of small volume elements have taken place. Glide packet formation in crystals strained at slow elongation rates results in diffraction maxima in X-ray patterns which are discrete points, and these discrete points indicate a few degrees of rotation for each packet. As the size of rotating volume elements decreases, the diffraction maxima become convoluted. In the necked region, the diffraction maxima are smoothly and continuously streaked as a result of this uniform rotation of small volume elements throughout the length of the necked region. The fact that diffraction maxima are streaked demands that the size of rotating volumes must be smaller than the resolving limit of the technique used, estimated at about 1 μm. Therefore, the observed reduction in area must depend upon the rotation of existing volume elements and not upon the movement of dislocations over long distances that give rise to slip packets. This, however, would not be the case with respect to simple shear fracture which requires the activation of only one slip system and entails only simple macroscopic rotation.

Thus, the incorporation into the boundaries of the ends of a dislocation, which have sheared a volume element, results in the rigid relative rotation of the volume element with respect to the original matrix of cells. This fundamental process is only dependent upon the rate of dislocation motion and upon the movement of dislocations over short distances as opposed to the appreciable distances moved in the formation of

slip steps. The above is essential to the description of the deformation history of single crystals prior to fracture.

The volume element rotations, which describe the phenomenology of stage III hardening, are particularly significant in the description of the geometrical changes in the necked region of α-Fe single crystals. In order to establish the relationship between macroscopically observed rupture (100 pct reduction in area) and the dislocation microstructure, one must first consider the nature of the dislocation structures arising just prior to crack initiation and the disposition of dislocations which may in itself give rise to fracture initiation.

To date, various dislocation pile-up models have been the popular explanation for fracture initiation in clean metals. Zener[17] suggested that a pileup of dislocations against a "strong obstacle" could lead to the formation of a crack. Cottrell[18] proposed that in a bcc crystal, the following dislocation reaction could occur:

$$\frac{a}{2}[\bar{1}\bar{1}1] + \frac{a}{2}[111] = a[001] \qquad [1]$$

where a is the lattice parameter giving rise to a sessile dislocation. This leads to the assumption that the microcrack due to the pile-up of dislocations at this sessile dislocation forms in the (001) plane. Stroh[19] elaborated upon an idea postulated by Orowan,[20] namely that a subboundary may act as a stress raiser in the solid, by considering that if a part of a dislocation wall interacts with a strong obstacle while the other part is being pulled by the applied stress, a crack ensues.

The credibility of such explanations is questionable. The majority of pile-up mechanisms would necessitate a one-to-one correspondence between obstacles and voids which is not seen, and further experimental evidence concerning their importance in metals has been lacking.

Rather, it is our contention that some other microstructural feature, which is in itself a direct consequence of the observed reduction in area, may give rise to ductile fracture initiation in pure metals.[21]

CONCLUSION

The deformation behavior of α-Fe crystals strained in tension describes a complex rotation of coherent diffracting volume elements exhibiting a consistent behavior as required by the reduction geometry. The necking process is independent of elongation rate and remains uniform throughout the necked region of the crystal. The description of the fracture processes in these whiskers must find its basis in the rotating volume elements or their surrounding boundaries. The initiation of a crack during the process of rupture cannot be understood in terms of motion of many dislocations over large distances, rather, it is due to the small rotated volume element and its subsequent boundaries. This, then, must be the site where a detailed description of fracture begins.

ACKNOWLEDGMENTS

The support of this research by the Metallurgy Branch, Office of Naval Research is gratefully acknowledged.

REFERENCES

1. R. N. Gardner: MS Thesis, University of Virginia, Charlottesville, VA, 1975.
2. R. N. Gardner and H. G. F. Wilsdorf: *Proc. 4th Int. Conf. on Fracture*, T. M. R. Taplin, ed., vol. II, pp. 349-56, University Waterloo Press, Waterloo, Canada, 1977.
3. R. N. Gardner, T. C. Pollock, and H. G. F. Wilsdorf: *Mater. Sci. Eng.*, 1977, vol. 29, pp. 169-74.
4. R. N. Gardner: Ph.D. Dissertation, University of Virginia, Charlottesville, VA, 1977.
5. R. W. Bauer, R. N. Gardner, R. L. Lyes, Jr., T. C. Pollock, and H. G. F. Wilsdorf: *Proc. of U.S. Japan HVEM Seminar*, pp. 102-05, Honolulu, HI, 1976.
6. T. C. Pollock: Ph.D. Dissertation, University of Virginia, Charlottesville, VA, 1977.
7. R. N. Gardner: *J. Cryst. Growth*, 1978, vol. 43, pp. 425-32.
8. R. N. Gardner and R. H. Hanscom: *Mater. Sci. Eng.*, 1976, vol. 22, pp. 167-70.
9. A. Luft, J. Richter, K. Schlaubitz, Ch. Loose, and Ch. Mulhaus: *Mater. Sci. Eng.*, 1975, vol. 20, pp. 113-22.
10. W. L. Piotrowskii: Ph.D. Dissertation, University of Virginia, Charlottesville, VA, 1965.
11. F. Guiu: *Phys. Status Solidi*, 1968, vol. 25, pp. 189-202.
12. H. L. Prekel, A. Lawley, and H. Conrad: *Acta Met.*, 1968, vol. 16, pp. 337-45.
13. K. R. Evans and E. B. Schwenk: *Acta Met.*, 1970, vol. 18, pp. 1-8.
14. D. Kuhlmann-Wilsdorf: *Work Hardening*, J. P. Hirth and J. Weertman, eds., pp. 97-139, Gordon and Breach, NY, 1968.
15. D. Kuhlmann-Wilsdorf: *Trans. TMS-AIME*, 1962, vol. 224, pp. 1047-61.
16. S. P. Agrawal, G. A. Sargent, and H. Conrad: *Met. Trans.*, 1974, vol. 5, pp. 2415-22.
17. C. Zener: *Fract. Metals*, p. 3, ASM, Cleveland, OH, 1948.
18. A. H. Cottrell: *Trans. TMS-AIME*, 1958, vol. 212, pp. 192-203.
19. A. N. Stroh: *Phil. Mag.*, 1958, vol. 3, pp. 597-606.
20. E. Orowan: *Dislocations in Metals*, p. 69, AIME, NY, 1954.
21. R. N. Gardner and H. G. F. Wilsdorf: *Met. Trans. A*, 1980, vol. 11A, pp. 659-69.

Ductile Fracture Initiation in Pure α-Fe: Part II. Microscopic Observations of an Initiation Mechanism

R. N. GARDNER AND H. G. F. WILSDORF

METALLURGICAL TRANSACTIONS A
VOLUME 11A, NUMBER 4

Physical Metallurgy and Materials Science
APRIL 1980

Ductile Fracture Initiation in Pure α-Fe: Part II. Microscopic Observations of an Initiation Mechanism

R. N. GARDNER AND H. G. F. WILSDORF

α-Fe single crystals of high purity were strained to fracture by *in-situ* high voltage electron microscopy. This method permitted recording of events leading to the failure of the crystal at high magnifications. Specifically, observations were made regarding the first step in the fracture mechanism, namely the initiation of voids, which occurred after a dislocation pattern of cells had developed. The cell size was found to be a few tens of nanometers in diameter and, because of the small scale of the dislocation patterns, a direct observation of void initiation was not possible. However, the misorientation between cells could be determined by electron diffraction techniques leading to the conclusion that void initiation took place at cell walls and at the boundaries of deformation microtwins. The high energy of these interfaces is another factor supporting the above conclusion.

PROGRESS has been made in the past decade with respect to the elucidation of the fundamental aspects of ductile fracture. The fibrous mode of ductile fracture, often termed microvoid coalescence, is known to proceed through the sequence of initiation, growth, and coalescence of voids.

The initiation of voids in the fibrous mode of fracture has in the past been solely associated with the presence of inclusions or particles in a multiphase alloy system. Mechanisms have been proposed whereby initiation sites are thought to be due to dislocation interactions at the particle-matrix interface, or, slip-induced fracture of a second phase particle.[1,2] Numerous reviews concerning particle fracture have been completed and are available in the literature.[3-7] This communication reports experimental findings with respect to essential aspects of the initiation process in pure α-Fe, and offers alternative mechanisms for ductile fracture initiation.

The first direct evidence for crack initiation in precipitate-free crystals was obtained as a result of *in-situ* studies in the high voltage electron microscope (HVEM).[8,9] Although additional studies have been completed in support of this conclusion,[4,10-12] in general, the implications of the results of these investigations with respect to their importance to ductile fracture may not have been fully comprehended or appreciated.

One issue which has long been controversial concerns the state of stress at the point of failure initiation in ductile "thin sheet specimens." The difference in fracture mode between bulk crystals and thin foils have been comprehensively investigated[13] and it has been demonstrated that void formation is taking place regardless of specimen thickness. Further, in the case of rupture (which is invariably preceded by severe necking in ductile metals) or indeed in the case of any test specimen under the conditions of a uniaxial stress, a reduction in area will give rise to triaxial stress conditions in the necked region.[14,15] Hence, a triaxial state of stress exists in those regions of samples where void initiation takes place and in fact one expects that these stress conditions may well be essential to the formation of the final dislocation structure found at the initiation of fracture.

Another point of apparent confusion is the distinction between the failure modes of simple shear fracture and rupture. The former failure mode does not require the participation of precipitate particles, and true void initiation does not occur in a sample failing due to simple shear. On the other hand, ductile rupture is a more complex phenomenon and this paper deals with the complex dislocation arrangements responsible for this mode of failure as interpreted from the *in-situ* investigation conducted.

A further comment concerning the nature of these *in-situ* fracture studies is appropriate to this last point. Generally, most investigators studying microstructural effects on fracture initially strain a crystal to fracture, then section the sample prior to recording the dislocation arrangements present. Consequently, information regarding the dislocation patterns present within the narrow region of the shear band is not obtainable when using such a technique. Hence the advantage of the *in-situ* study of fracture is that one is not limited merely to information from outside the region of greatest dislocation activity, *i.e.*, from outside the shear band.

EXPERIMENTAL

Techniques employed in the growth and characterization of crystals have been described elsewhere.[16]

The preparation of samples for the *in-situ* investigations involved mounting the filaments on copper supports. These copper supports, prepared by a photofabrication process similar to the one outlined by Lyles,[17] not only serve as a means of holding the small crystals, but also provide a way in which to transmit a uniaxial stress to the whisker. Single crystals were glued to the copper supporting grid; specifically, a polymer resin manufactured by Bakelite Company and soluble in cyclohexanone ($C_6H_{10}O$) was used.

Tensile supports were placed in a hydraulically

R. N. GARDNER is Senior Research Scientist, 3M Company, 3M Center, Central Research Laboratories, St. Paul, MN 55101, and H. G. F. WILSDORF is Wills Johnson Professor of Materials Science, School of Engineering and Applied Science, University of Virginia, Charlottesville, VA 22901.

Manuscript submitted October 16, 1978.

ISSN 0360-2133/80/0411-0659$00.75/0

loaded tensile apparatus designed and built for use in a RCA 500 kV HVEM. This tensile stage is similar in design to that constructed by Wilsdorf.[18] The hydraulic system was fully enclosed to alleviate an earlier problem caused by the presence of air bubbles admitted into the system, which in turn had resulted in variations in the elongation rates of tensile specimens.

Dynamic studies involving direct observation of *in-situ* fracture were recorded on videotape at a viewing speed of thirty images per second. The recorder was coupled with a low light level image intensifier. The elements of this monitoring system have been reviewed elsewhere.[3,17]

All transmission microscopy was performed using an accelerating voltage of 500 kV, and 250 μm condenser aperture. All micrographs were taken during dynamic, *in-situ* fracture. Objective apertures used ranged in size, the smallest being a 5 μm aperture which was utilized in order to compensate for the observed losses in image contrast due to the high accelerating voltage of the electrons.

Micrographs have been shown in an earlier publication which are representative of transmissionable crystals that were obtained from some of the "controlled" growth runs performed.[16] Due to variations of nucleating surfaces, the external geometries of crystals were regulated with precision by the controlled addition of small amounts of oxygen during growth. The resulting whiskers are transmissionable and of a ribbon-like geometry which has been shown to be ideal for *in-situ* HVEM fracture experiments, in particular because transmissionable crystals do not require preparation techniques such as electrolytic thinning and ion milling which can damage samples.[19] In contrast, the micrographs depicted in this communication are of "prepared" crystals, 4 to 5 μm in thickness (hence they were not initially transmissionable) in order to be able to draw analogies from a complete microstructural analysis of bulk, 3-D crystals after deformation as applied to "real" materials.

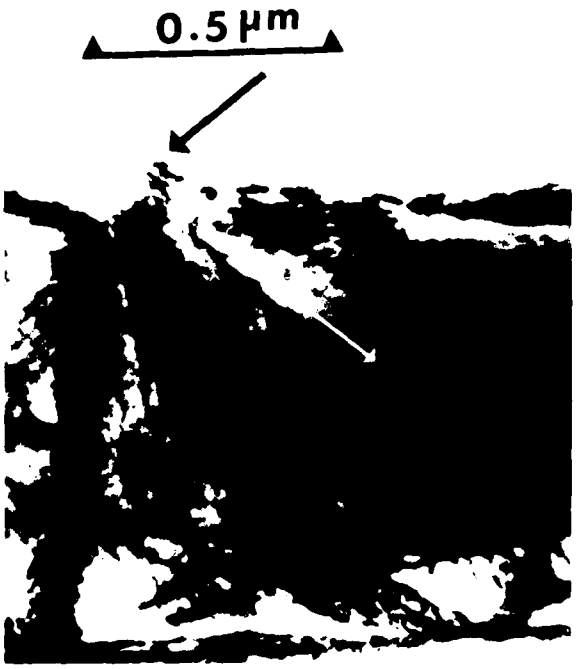

Fig. 1—Representative HVEM micrograph (500 kV) displaying cells at the crack edge (dark arrow) which became difficult to discern in the thicker regions of the crystal (light arrow).

RESULTS

More than sixty crystals were examined during *in-situ* straining in the HVEM. These samples were initially examined by shadow contrast. As the crystals became transmissionable during straining, it was noted that the dislocation density was extremely high. However, at higher magnifications, networks of dislocations could be imaged and existing layers of networks which were present even to the very ends of the crack flanks were observed.

Figure 1 is typical of the network structures seen and displays cells of about 15 nm in size. In this micrograph it is noticeable that the networks of cells are indeed continuous to the edge of the crack flank. The point designated by the black arrow is the thinnest region of this crystal. Proceeding from the edge of the crystal into the thicker region of the specimen, layer upon layer of cells still satisfy the conditions for diffraction contrast and hence imaging of descrete cell boundaries becomes difficult. High dislocation densities and small cells such as these are the reason that it is difficult to determine the nature of the braided or lacey contours at high deformations.[20] The layers of cells mentioned above can cause periodicities in intensities that are observed in the form of fringes (Fig. 2). Selected area diffraction (SAD) patterns were taken of the areas noted in Fig. 3.

At this point, it might be mentioned that in a general field of extinction contours, a periodic extinction of the transmitted wave, in this case due to foil bending, appears as in Fig. 4(*a*). The extinction distances for low order reflections are about a few tens of nanometers and increase with increasing order of reflection. A rotation of a volume element about the long axis of the contour leads to the displacement of part of the contour. Numerous displacements of this type result in the appearance of 'braided contours.'

Selected area diffraction patterns were taken to ascertain the character of the microstructure under examination. Analytical methods for calculating diffraction patterns containing twin reflections are available in the literature.[21-23] However, when patterns do not contain simple twin relationships, these methods can become cumbersome. The method employed by the authors is that as outlined by Kelly[24] and reviewed by Edington,[25] involving the use of twin stereograms. The process entailed the indexing of all major types of zone axis patterns appearing on a diffraction pattern. It then became necessary to locate these on a twin stereogram; to calculate the correct orientation relationships between patterns, and finally to identify any double diffraction spots if present.

Figure 5 is representative of the SAD patterns taken of the crack flanks shown in Fig. 3. The area encompassed by the SAD aperture is approximately 500 nm average angles of rotation are about 20 deg, and the presence of deformation twins is apparent. A large number of crystals were observed to have such deformation twins. The determination of Fig. 5(*a*) required

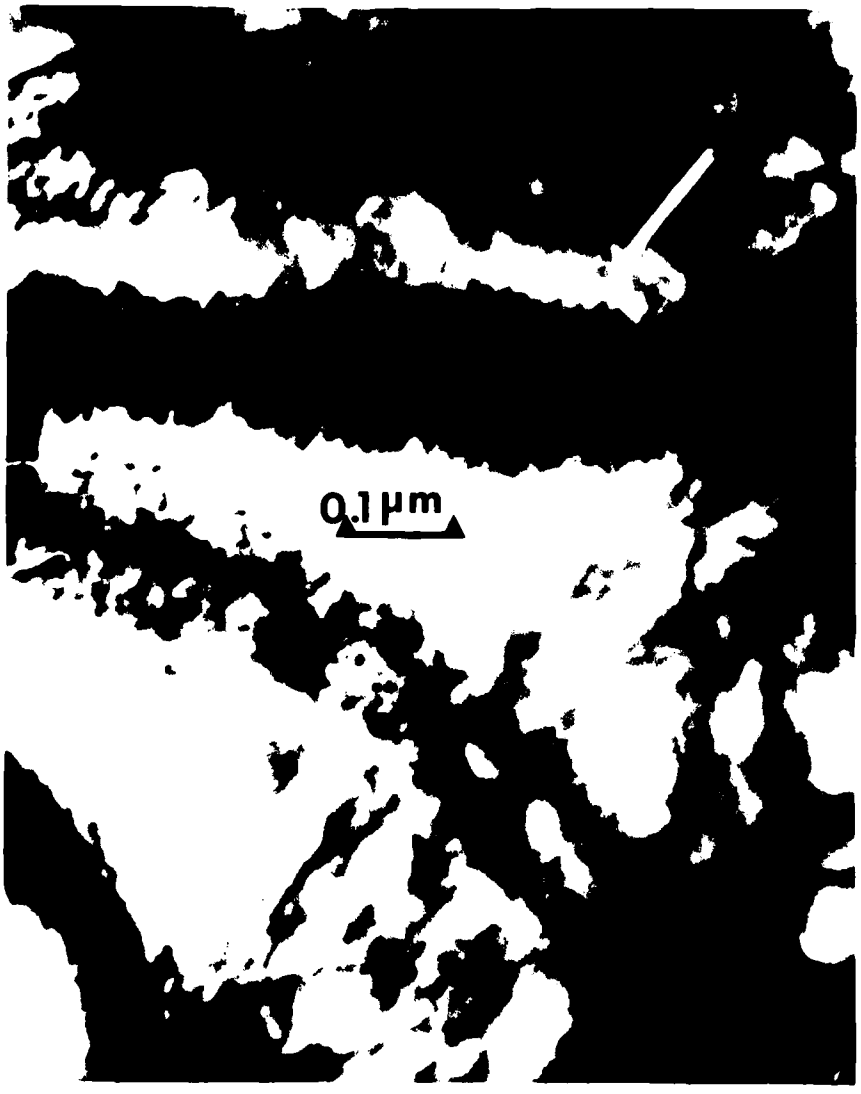

Fig. 2—The arrow denotes parallel fringes, indicative of overlying repetitive microstructures identified in Fig. 1 as small cells. Other interesting patterns displaying some periodicity of contrast are observed in the contours of this micrograph (HVEM, 500 kV).

the overlay of various separate patterns to form the composite patterns ultimately achieved in Fig. 6. In this particular pattern, overlaying ⟨311⟩ and parallel ⟨511⟩ patterns, as well as radial asterism of diffraction maxima, indicate the degree of cell rotations. The $(0\bar{1}1)$ spot of the [311] zone axis pattern may be transformed by twinning about the $(\bar{1}12)$ to form the $(1\ 3\ -4/3\ 1\ 3)$ spots of a twinned matrix. The relationship between the matrix pattern and the new zone axis pattern of the twin can be found by taking the dot product of the two unit vectors. That is, for $(\mathbf{A}\cdot\mathbf{B})\ (\mathbf{AB})\ \cos\phi$ one obtains ϕ 33.29 deg.

A few degrees off the reflecting zone axis is the ⟨114⟩ zone axis. Deformation twinning of this zone axis may appear on the pattern. The reflections of the ⟨114⟩ zone axis form a parallel pattern with the original ⟨113⟩ and ⟨115⟩ zone axes reflections. Hence, perpendicular to the $[1\bar{1}0]$ direction, among the spots of the pattern would appear the $(44\bar{2})$ spot. Twinning of this spot would give rise to the (002) spot and the subsequent overlaying zone axis pattern would be the [110]. The (002) spot would then be oriented 110 deg from the perpendicular of the [110] direction in the original [113] zone axis patterns. Hence, the appearance of a parallel [331] zone axis pattern which is parallel to the [110] zone axis pattern results from rotation that is attributable to deformation. Slip, then, has preceded the formation of deformation twins and continues after twinning has taken place. This is in agreement with the findings of a study by Mahajan[26] on deformation twinning in a Mo-35 at. pct Re alloy.

Figure 5(*b*) displays spots resulting from discrete maxima. Most streaking recorded by electron diffraction is spotty. This pattern is indexed in Fig. 7. Zone axis patterns again have twin relationships. The pattern taken of area C in Fig. 3 is displayed in Fig. 8. The d_{hkl} spacings are all indexed; much streaking is observed.

An additional representative example of the crack flank of these crystals is given in Fig. 9. Fig. 10 displays contours composed of a network of cells. SAD patterns were taken at different positions; these are

shown in Fig. 11(*a*) through (*c*). Because of the small size of filaments, it was not possible to place them in a tilt stage after fracture and so only slight tilting was done and the rotations are limited. However, a great deal of information may still be gained by examination of the diffraction maxima. Figure 11(*a*) shows a SAD pattern which was taken when the foil orientation was close to the ⟨111⟩ zone axis, and the figure displays overlaying patterns, some possibly due to volume rotations. In the case of a volume element oriented with its [111] axis parallel to the electron beam, the twinned region would be oriented either along the [115] or along its [111] direction, depending upon the specific composite plane of the twin, (112) or (11$\bar{2}$) respectively.[27] In either case, twin spots would overlap the matrix spots and one could not differentiate between the two. However, the formation of the (03$\bar{1}$) twin spot and an overlaying [331] foil axis pattern was observed. If (03$\bar{1}$) is attributed to a twinned volume, then the twinned material is oriented along its [115] axis. This results

Fig. 3 Diffraction patterns were taken from the regions marked.

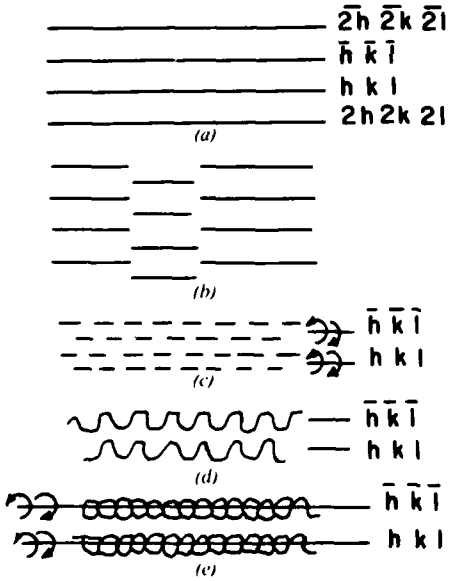

Fig. 4 The schematic drawing represents the formation of 'braided' or 'lacey' contours. (*a*) A general field of extinction contours may result from bending of the foil and is due to a periodic extinction of the transmitted wave. (*b*) The rotation of a region of the diffracting sample about the long axis of the contour results in the uniform displacement of contours. (*c*) Many such rotations may occur and when the rotating volume elements are small in size, it may be difficult to distinguish between individual contours which result. This effect eventually results in the serpentine appearance of contours, as illustrated in (*d*). (*e*) Finally, layers of rotated cells will give rise to the 'braided' appearance of contours. This effect occurs when small dislocation cells are present.

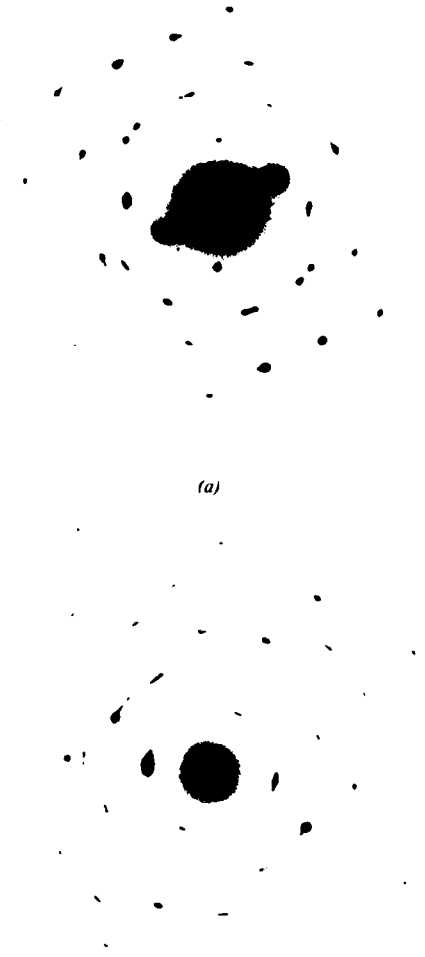

Fig. 5 Representative of selected area diffraction patterns taken of the crack flanks. (*a*) This pattern is completely determined in the following series of figures. (*b*) Note that the diffraction maxima are a discrete array of spots. All spots have d_{hkl} spacings attributable to bcc iron.

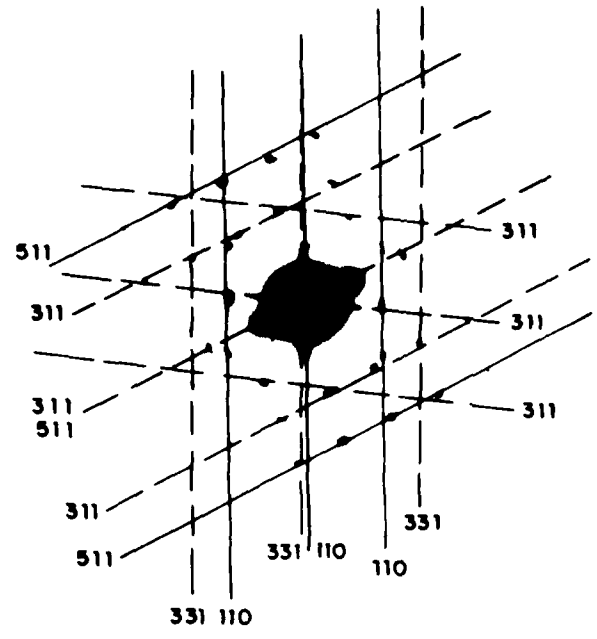

Fig. 6—Electron diffraction pattern of Fig. 5(2) with zone axis patterns drawn in.

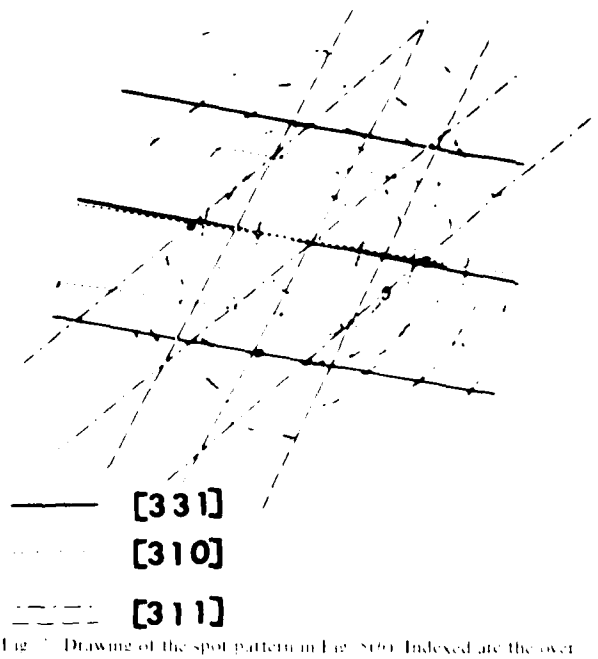

Fig. 7—Drawing of the spot pattern in Fig. 5(b). Indexed are the overlaying zone axis patterns found in the diffraction pattern.

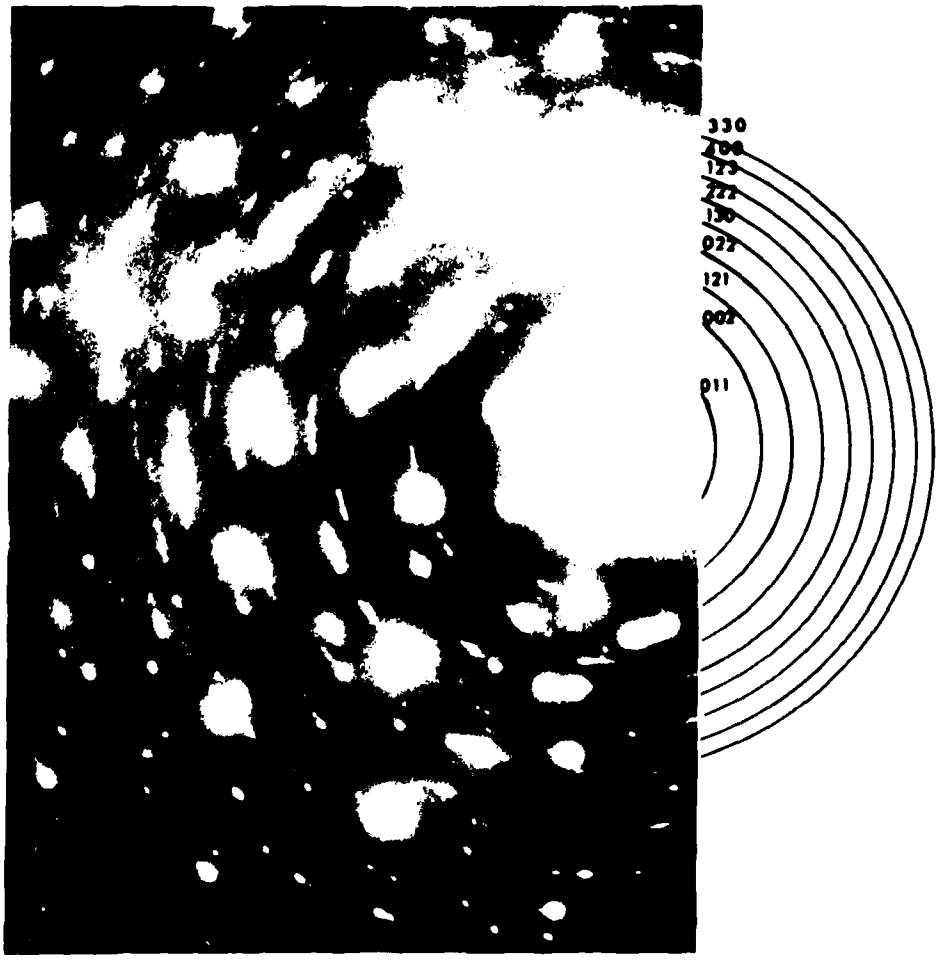

Fig. 8—Selected area aperture allows diffraction from an area of about 0.8 μm in diam. The pattern is most probably the result of about 500 to 1000 cells and appears similar to a textured polycrystalline pattern.

from the fact that the $[03\bar{1}]$ pole falls about 7 deg from the (115) basic circle on the back side of the reference sphere. Spots indexed 4 3 ($0\bar{1}1$) and 1 3 ($\bar{4}15$) in Fig. 12 may arise from the diffraction of the ($03\bar{1}$) twin spot from the ($01\bar{1}$) and ($\bar{1}21$) points of the matrix.

Other anomalous spots may also be explained in a similar manner. Therefore, what has been formed is an apparent $[331]$ beam axis pattern over the $[111]$ matrix pattern (Fig. 13). (110) spots near those which form part of the $[331]$ pattern may belong to a 100 pattern. Spots indexed as 4 3 ($0\bar{1}1$) and 1 3 ($\bar{4}15$) may compose the rest of the 100 pattern. The 100 pattern must be due to the rotations of the 115 zone axis about the 110 as shown in Fig. 14. This can only occur if plastic deformation has taken place after the twin volume has formed. As one might expect, the appearance of (110) spots 90 deg to ($01\bar{1}$) spots suggest that ⟨011⟩ is the axis of rotation of the (115) zone axis pattern.

In Fig. 11(*b*) and (*c*), large continuous volume rotations appear in the ⟨110⟩ zone axis pattern, while in the ⟨100⟩ zone axis pattern a tendency towards an overlaying pattern is seen. These series of patterns are indicative of the same type of patterns obtained from the precession method.[28] The X-ray precession method is a nondestructive and easy-to-interpret record of the deformation process as it is a direct enlargement of the reciprocal lattice. As opposed to representing only a "selected area", rather it represents an averaging affect over a large volume. Specifically, then, as the preceding presentation of diffraction analyses indicated, large volume rotations, overlaying zone axis patterns, and twinning as observed in this study are consistent with the results obtained from both the X-ray precession method and the electron diffraction patterns.

During *in-situ* straining experiments, pinholes were observed to form at various points along the width of the ribbons, within the narrow region along the length of the sample that is the shear band. Pinholes and thin spots were on the order of a small cell in size, and were noticed to occur at cell boundaries. However, this phenomenon was, in general, photographed and observed by mass thickness contrast (Fig. 15).

If one now considers the resulting fractured end of a crystal, that during straining displayed voids and hole formation as observed by mass thickness contrast, the presence of holes in front of the cracked edge and a rather jagged foil crack flank becomes apparent by diffraction contrast (Fig. 16). Diffraction patterns of the area where holes are seen indicate little distortion. Along the region of the jagged foil, twin relationships are once again observed. Thus, both dislocation subboundaries as well as deformation twins were observed to be the initiation sites for microcrack formation.

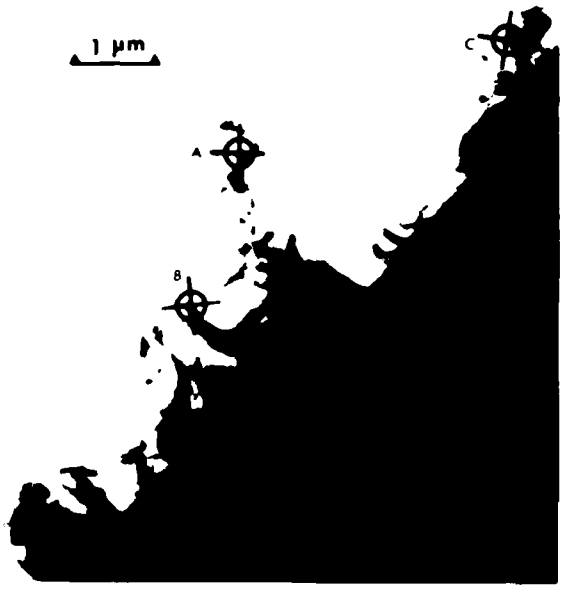

Fig. 9—Typical crack flank. Areas investigated further have been marked.

Fig. 10—(Area B) A fine network of cells is apparent along all contours.

(a)

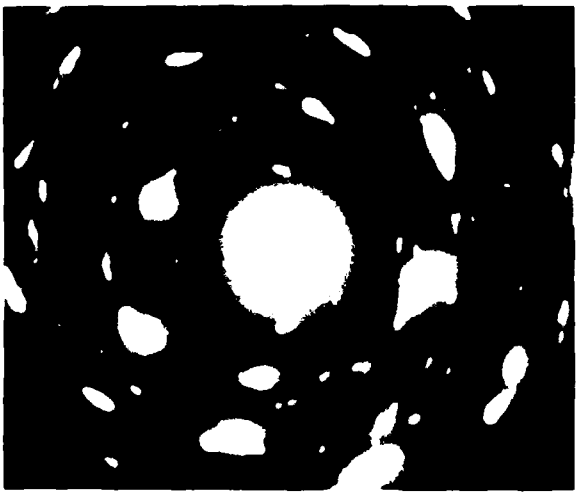

(b)

Fig. 11—SAD pattern of area A, B, and C in Fig. 9. Large, continuous volume rotations give rise to streaked diffraction maxima in B and C. Streaking as a result of double diffraction appears in both patterns.

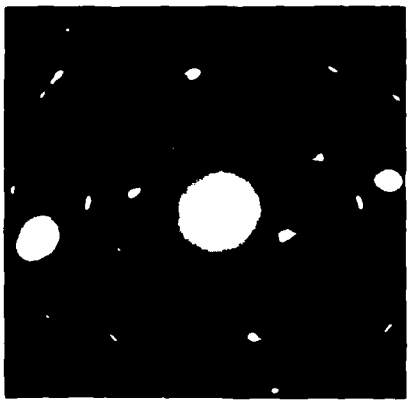

(c)

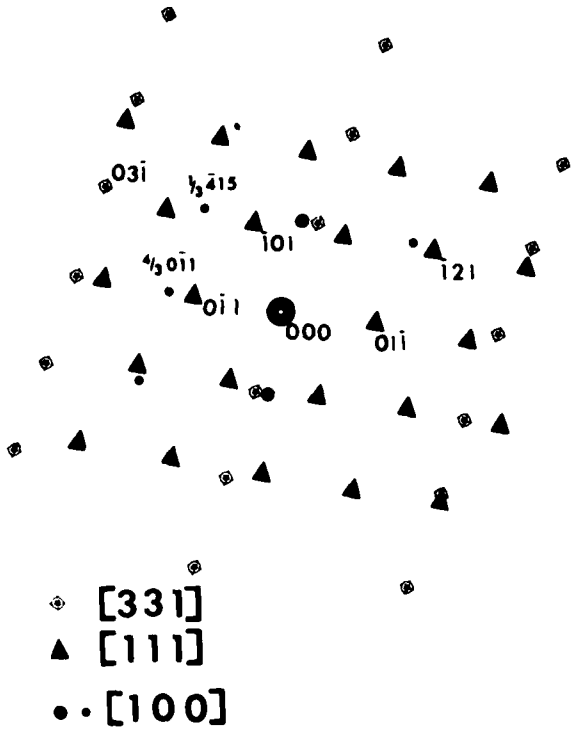

Fig. 12—The position of the spots indicates a number of possible overlaying patterns. As is demonstrated in Fig. 14, the appearance of the [100] zone axis pattern is as a result of volume rotation whereas the [331] pattern is a result of twinning.

DISCUSSION

The blueprint for ductile fracture may be considered to begin at the initiation of Stage II hardening and is related to subsequent sub-boundary formation.[29,30] The shear band is the site of greatest dislocation activity and hence the largest angle sub-boundaries are formed in the narrow region of the shear band. This concept requires the presence of relatively high angle boundaries only within the narrow region defined by the shear band and not over the entire necked portion of the sample. Observation of the crack flanks in the HVEM has provided information as to the state of sub-boundaries in the shear band at fracture.

Early in the deformation history of these crystals, dislocations move in such a manner that the stress field of each dislocation is "screened" from that of every other dislocation. Consequently, three-dimen-

sional networks of cells form in accordance with the meshlength theory of workhardening.[31,32] This initial dislocation pattern will shrink in size as a result of the principle of similitude.[33,34] However, complete similitude in single crystals is not necessary for the meshlength theory of workhardening to be applicable.

It is probable that this lack of homogeneity in cell shrinkage in single crystals and polycrystalline foils is responsible for the nonuniformity of boundaries that exists at sites of fracture initiation. Or, the nonuniformity in the strength of low angle boundaries observed in metals[20,35,36] might be ascribed to a mere statistical effect. In either case, the meshlength theory describes a cell pattern where cell components continue to shrink in size while at the same time they are increasing in continuity, thereby occupying a greater volume of metal. This process continues throughout Stage II hardening until a minimum cell size is achieved at the beginning of Stage III. At this point in the deformation process a generally continuous three-dimensional network of cells exist.

Stage III hardening may thus be described as resulting from the motion of dislocations through networks of cells. The incorporation of the dislocation into a cell wall causes rigid relative rotation of the cell's interior with respect to its surroundings. This is a geometric phenomenon of great consequence of fracture.

At this point, let us consider the apparent causes of fracture initiation at sub-boundaries. Fracture initiation at sub-boundaries occurs in the most highly deformed part of a tensile sample and is thus determined to be due to the dislocation structures which are formed late in Stage III hardening. The degree of deformation preceding Stage III depends upon several variables and differs from orientation to orientation, implying once again that large rotations or misorien-

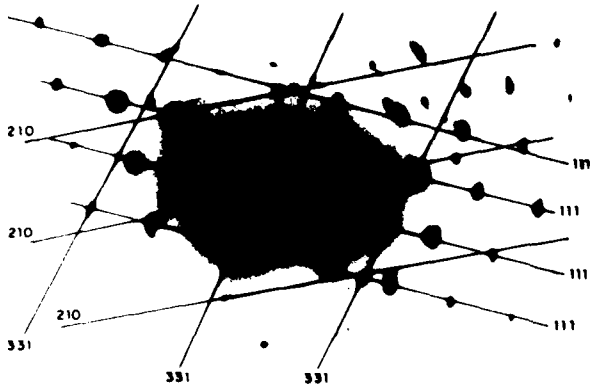

Fig. 13—Indexed pattern of Fig. 11(a). The (100) pattern is "washed out" here, but appears in Fig. 11(a), and has been depicted in Fig. 12.

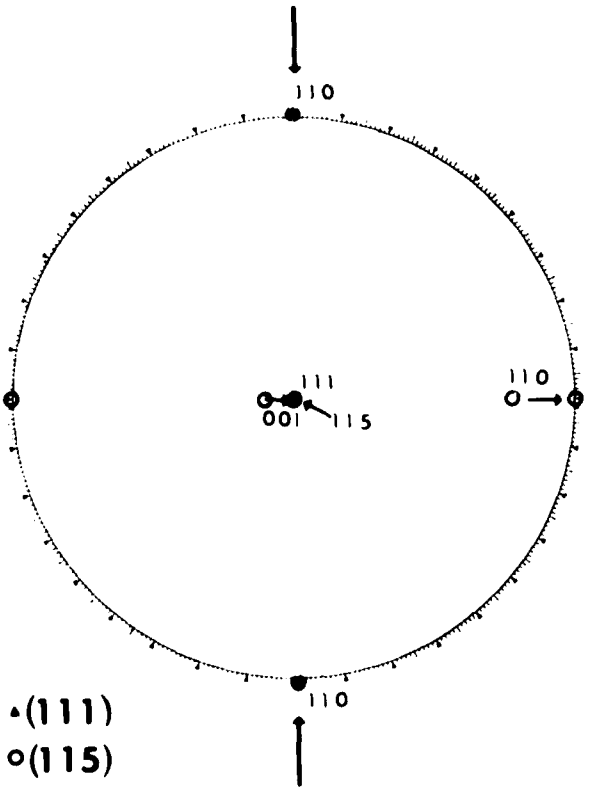

Fig. 14—Standard stereographic projection involving the superimposition of the (115) over the (111), indicating (arrow) the axes about which rotation has taken place to cause diffraction from those spots composing the (001) zone axis pattern and giving rise to the appearance of twin spots.

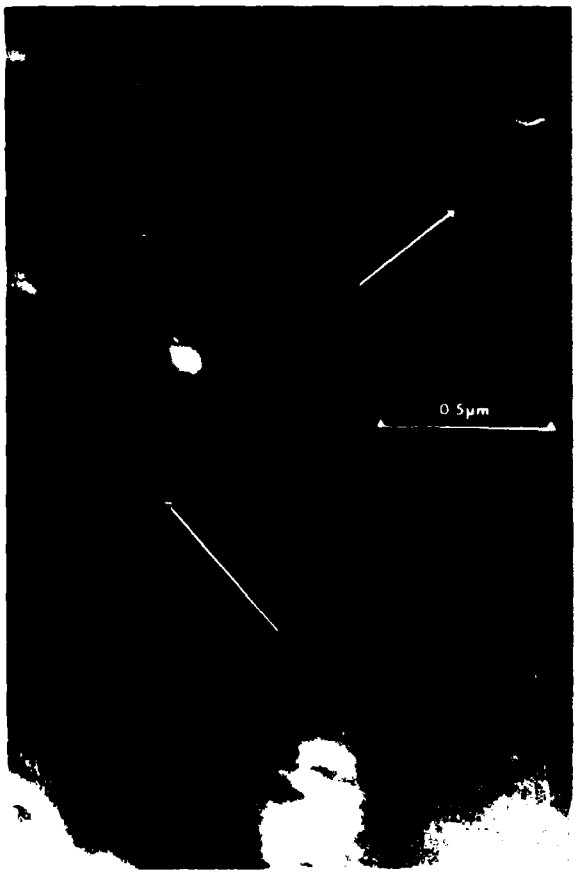

Fig. 15—Cracks of less than 0.4 μm were observed to open within the vicinity of the shear band. The unlabeled arrow designates the direction of the moving crack.

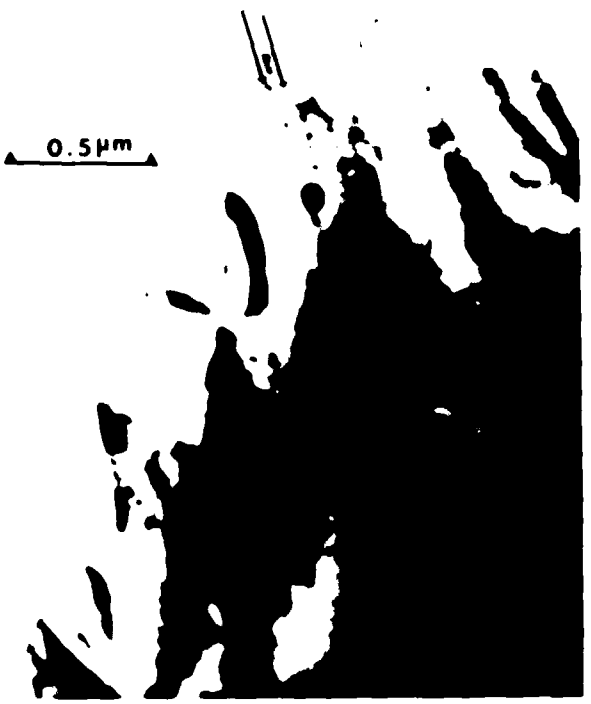

Fig. 1—Holes are apparent in this micrograph and are in diffraction orientations with by they appear both light and dark. A jagged edge is also observed.

tations in boundaries do not occur until late in the deformation process. Witcomb has observed that in Mo-50 at. pct Re, the reduction in the dislocation cell diameter was found to level off at 24 pct deformation (elongation). Thus, it is unlikely that high energy boundaries in bcc metals, which may serve as sites for fracture initiation, are formed until substantial plastic deformation of the sample has taken place. Recently, French and Weinrich[7] have determined in alpha-brass that void formation without the involvement of particles must occur in the final stages of deformation.

Hecker, Cox, and Stein[8] have observed fracture in Ir occurring at grain boundaries. They have shown, through the application of Auger analysis of samples fractured in high vacuum, that the segregation of impurities at grain boundaries did not take place, nor were there present any other second phase particles. Fracture of a clean grain boundary can and does occur.

Twin boundaries belong to a class of special low energy boundaries known as coincidence boundaries, because the twin-related crystals share a specific number and arrangement of coincidence sites. Whether the boundary is a special coincidence-boundary, high angle boundary, or a general dislocation sub-boundary, it invariably represents a site of higher energy than the trivial case of two crystals aligned such that there is no misorientation across their interface, *i.e.*, a one-to-one correspondence between atoms as in a perfect crystal. Grain boundary energy vs increasing relative angle of misorientation is seen to range from 0 to 600 (mN/m) in Cu [100] tilt boundaries. For misorientations of ⟨110⟩ Ni grains, 900 (mN/m) is the energy at about 20 deg of misorientation.[40]

The existence of dislocation cells, as well as the occurrence of cell rotations in samples subjected to stresses as great as their ultimate tensile stress are phenomena which correspond well with the findings of other studies. Langford and Cohen[35] in their experiments with heavily deformed iron wire, discovered that cells had formed and were present in samples which underwent as much as a 99.9 pct reduction in their original cross-sectional areas. They found misorientations between cells of about 15 to 20 deg.[20] In a microstructural analysis of severely drawn iron wires, Langford and Cohen found that there were varying values and distributions for angles of misorientation, which were related to the degree of work-hardening. A statistical variation in the strength of boundaries was observed. Thus, there are sub-boundaries whose angles of misorientation, or strengths, are approximately the same as those of typical grain boundaries. Their work was also evidence for an increase in width of the distribution of angles of misorientations with increasing wire drawing strain. At a true strain of 7 the authors found that cells and grains were indistinguishable.

The physical limitations of this *in-situ* HVEM study were due to the small cell sizes. It has not been possible to determine the exact distibution in angular misorientation. Langford and Cohen have stated that their approach may be applied to cell sizes of 50 nm if the accelerating voltage was about 1100 kV.[20] The minimum cell sizes they studied were 0.1 μm, at an accelerating voltage of 800 kV. The 20 nm cell size seen in this effort did not allow for such an eloquent study.

Consider, then the case of one boundary separating two volume elements that are rotated about a common axis. The incorporation of dislocations, which have sheared the adjacent volume element, into the boundary continues to increase the relative misorientation of the boundary.

E_f is defined as the energy of fracture necessary for decohesion across this or any interface. For a metal of single phase, this is merely equivalent to the energy of adhesion given by:

$$E_f = 2\gamma_s - \gamma_b \qquad [1]$$

where γ_s is the surface energy and γ_b is the energy of the interface or boundary under discussion. For perfect registry of contacting surfaces, $\gamma_b = 0$, representing the trivial case where the work necessary to cause fracture is equal to the surface energy of the new surfaces created. It is apparent that the increase in γ_b that results during cell rotation lowers the amount of work necessary for fracture, or decohesion of the boundary involved, to occur. Therefore, at high stress levels the boundary having the largest value of γ_b is a preferred site for microcrack nucleation. Thus, it is seen that initial crack formation at sub-boundaries will be energetically favored over any impurity-free interface chosen within the cell. It is not surprising that crack initiation should take place at cell walls in the absence of second phase particles, when one considers the corresponding decohesion energy for fracture. L. E. Murr has tabulated ratios of the grain boundary-to-solid vapor free energy.[10] Values range from about 0.25 to 0.45, and were taken at relatively

high temperature. This suggests that the energy for fracture may be reduced by as much as 25 pct.

To the above simple considerations, it may be added that the degree or relative misorientation which the crystal is able to accommodate before failure occurs, is somewhat dependent upon the strain rate imposed on the sample.[11] However, these variations will probably only be of importance to dynamic shock loading, which is not being considered here.

Having studied the relative energetics of crack initiation at sub-boundaries, the expected position of these boundaries with respect to the test sample may be examined. It is as a consequence of the dynamics of dislocations describing this event that the largest dislocation motion causing an increase in the energy of the boundary will occur along the predicted shear band. This is necessarily due to the fact that dislocation motion during plastic deformation is largely dependent upon shear stresses. Thus, once nucleated, a crack propagating along the shear band is actually preceded by other microcracks which are at the same time nucleating at sub-boundaries just ahead of the crack front. This phenomenon has been substantiated by the findings of other investigators, who report cracks opening along the shear band at the same time and ahead of the primary crack.[11,12]

One can identify the nature of the stresses that are present at fracture by close inspection of the edges of the crystal in Fig. 1 where one sees the "triangular" appearance of cells. Irregularly shaped cells indicate that relaxation has not yet occurred in these areas.

Models that have been used to explain crack formation due to twins are based on stress concentrations due to dislocation pile-ups at obstacles such as a grain boundary,[12,13] twin boundary;[14] or, due to the intersection of two twins,[15-17] due to the combination of the slip dislocations producing $a_0\langle 001\rangle$ dislocations[18] or finally, due to a reaction between emissary slip dislocations.[19] Additional models describe cleavage as the result of the fracture of a deformation twin[50,51] or explain that failure occurs as a result of a shock wave which is radiated when a twin strikes an obstacle.[52]

Here again one suspects that the decohesion of the twin boundary initiates a crack. This occurrence may be described as a pseudocleavage crack in that it may occur in an abrupt fashion. Decohesion of the energetically favored boundary can occur at a speed limited only by the rate of propagation of the last dislocations which are incorporated into the boundary, providing the minimum energy for decohesion at the boundary interface.

An initial crack has now been formed, and the linking of microcracks formed at sub-boundaries may be described either by the movement of a large number of vacancies from nearby boundaries (as a reaction to large stress fields) or by dislocation activity. Previous studies have implied that dimple density or crack spacing is dependent upon strain rate.[3] This may suggest a vacancy mechanism, but it is most probably due to a strain rate dependency of the cell size.

SUMMARY

The presence of twins in these crystals is directly related to their ultimate tensile strength. The iron whiskers examined in this study exhibited ultimate tensile stresses as high as 10^9 Pa at room temperature. Similar values of fracture stress have been reported by Allen, *et al* for iron single crystals of 99.96 pct purity, which failed by cleavage at low temperatures.[53] Allen further observed the same range of nucleating stress for twins at low temperatures as has been observed in this effort. This is important because twinning in bcc metals at room temperature has previously been reported only in substitutional solid solution alloys where a low stacking fault energy exists and has generally been associated with the nucleation of deformation twins by some investigators.[54] It appears then that twinning in these crystals may obey a critical resolved shear stress law.

The crystallographic character of fracture planes displayed by the single crystals upon failure inherently depends upon dislocation processes leading to fracture and hence arises from substructures which have evolved during deformation. These fracture modes remain at all times microscopically crystallographic often giving rise to fracture geometries which appear even macroscopically crystallographic. Clearly, these crystals are not failing due to a simple shear process.[55]

Characterization of the deformation history preceding fracture of these crystals has revealed that the geometry of reduction in area, as well as the work-hardening rates of these crystals are *dependent* upon the number of active slip systems.[29] On the other hand, the whiskers' geometry of reduction in area, a predictable property of crystal orientation, is *independent* of elongation rate, unlike slip trace depth.[29] The rotational behavior observed is reminiscent of that found in the formation of bcc textures.[56] Specifically, it is observed that as a consequence of the activation of slip systems having $\langle 111\rangle$ Burgers vectors, the once highly oriented sample displays much streaking of diffraction maxima about a $\langle 111\rangle$ texture axis.

The evolution of dislocation structures necessary to accommodate the geometric reduction in area is such that small volume elements form. These volume elements, although too small to be resolved by simple X-ray diffraction techniques, are directly observed in the HVEM to be dislocation cell structures that exist throughout the late deformation stages and fracture itself. Since the geometric reduction in area is uniform despite any possible variations in strain rate, then the accommodation of large strains as well as the reduction in area must be determined by the movements of dislocations on the order of distances equal to those of the dislocation cell size. In addition, since sharp straight chisel edges are not observed in the fractured ends of the crystal, but rather very ragged edges, this implies that microstructures present in the neck of the crystal, specifically boundaries and microtwins, provide initiation sites for fracture. Detailed diffraction analysis has demonstrated that considerable misorientation between dislocation cells exists as a result of deformation. Thus, voids initiating late in the stages of ductile fracture initiate due to decohesion at high angle, high energy sub-boundaries and twin boundaries as has been observed in the HVEM.[30,57] The presence of precipitate particles therefore is a sufficient but not a necessary condition for ductile fracture initiation.

Since the completion of this investigation, microcrack formation at cell walls has also been observed directly

in the HVEM, in single crystal Be,[30,57] giving further support to the conclusions of this study. In Be (hcp), the stacking fault energy is lower than that found in α-Fe (bcc) and one would expect larger cell sizes. These larger cell sizes are clearly advantageous in the HVEM in that they allow for better imaging of *in-situ* crack initiation at the lower magnifications necessary for *in-situ* experiments.[30,57] In addition, T. Imura has shown microcrack initiation at cell walls in a movie on *in-situ* plastic deformation of iron (Ref. 58) and H. Fujita has communicated the occurence of similar phenomena in aluminum.[59] It is apparent, then, that the process of decohesion at sub-boundaries is fundamental to the mechanism of mechanical failure of heavily workhardened pure metals.

ACKNOWLEDGMENTS

The support of this research by the Metallurgy Branch, Office of Naval Research, is gratefully acknowledged.

REFERENCES

1. J. Gurland: *Trans. TMS-AIME*, 1963, vol. 227, pp. 1146-50.
2. J. T. Barnby: *Acta Met.*, 1967, vol. 25, pp. 903-09.
3. R. W. Bauer: Ph.D. Dissertation, University of Virginia, Charlottesville, VA, 1975.
4. D. Broek: Ph.D. Dissertation, Tech. Hogeschool Delft, Netherlands, 1971.
5. J. R. Low: *Fract. Mech.*, 1968, vol. 1, p. 47.
6. A. R. Rosenfield: *Met. Rev.*, 1968, vol. 121, pp. 29-40.
7. D. R. Curran, Lynn Seaman, and D. A. Shockey: *Phys. Today*, 1977, vol. 30, no. 1, pp. 46-55.
8. R. W. Bauer, R. H. Geiss, R. L. Lyles, Jr., and H. G. F. Wilsdorf: *Jernkont. Ann.*, 1971, vol. 155, p. 403.
9. R. W. Bauer, R. H. Geiss, R. L. Lyles, Jr., and H. G. F. Wilsdorf: *Proc. 29th Ann. Meeting Elec. Micro. Soc. Am.*, p. 130, Clayton's Publishing Division, Baton Rouge, LA, 1971.
10. R. W. Bauer and H. G. F. Wilsdorf: *Scr. Met.*, 1973, vol. 7, pp. 1213-20.
11. J. A. Alic and R. M. Asimow: *Eng. Fract. Mech.*, 1972, vol. 4, pp. 915-23.
12. R. L. Lyles and H. G. F. Wilsdorf: *Acta Met.*, 1975, vol. 23, pp. 269-77.
13. R. W. Bauer and H. G. F. Wilsdorf: *Proc. Int. Conf. on Dynamic Crack Propagation*, G. C. Sih, ed., pp. 197-213, Noordhoff Int. Publishing, Leyde, 1973.
14. G. E. Dieter: *Mechanical Metallurgy*, p. 344, McGraw Hill, New York, NY, 1976.
15. D. A. Ryder, T. J. Davies, I. Brough, and F. R. Hutchings: *Metals Handbook*, H. E. Boyer, ed., vol. 10, p. 19, ASM, Ohio, 1975.
16. R. N. Gardner: *J. Crys. Growth*, 1978, vol. 43, pp. 425-32.
17. R. L. Lyles, Jr.: MS Thesis, p. 146, University of Virginia, Charlottesville, VA, 1971.
18. H. G. F. Wilsdorf: *Rev. Sci. Instrum.*, 1958, vol. 29, pp. 323-24.
19. R. N. Gardner: Ph.D. Dissertation, University of Virginia, Charlottesville, VA, 1977.
20. G. Langford and M. Cohen: *Met. Trans. A*, 1975, vol. 6A, pp. 901-10.
21. E. S. Meieran and M. H. Richman: *Trans. TMS-AIME*, 1963, vol. 227, pp. 1044-46.
22. O. Johari and G. Thomas: *Trans. TMS-AIME*, 1964, vol. 230, pp. 597-99.
23. C. M. Wayman and R. Bullough: *Trans. TMS-AIME*, 1966, vol. 236, pp. 1711-15.
24. P. M. Kelly: *Trans. TMS-AIME*, 1965, vol. 233, pp. 264-65.
25. J. W. Edington: *Practical Electron Microscopy in Materials Science*, MacMillan Phillips Technical Library, Eindhoven, Netherlands, 1977.
26. S. Mahajan: *Phil. Mag.*, 1972, vol. 26, pp. 161-71.
27. S. Mahajan: *Phil. Mag.*, 1969, vol. 19, pp. 99-204.
28. R. N. Gardner and R. B. Hanscom: *Mater. Sci. Eng.*, 1976, vol. 22, pp. 167-70.
29. R. N. Gardner and H. G. F. Wilsdorf: *Met. Trans. A*, 1980, vol. 11A, pp. 653-58.
30. R. N. Gardner, T. C. Pollock, and H. G. F. Wilsdorf: *Mater. Sci. Eng.*, 1977, vol. 29, pp. 169-74.
31. D. Kuhlmann-Wilsdorf: *Trans. TMS-AIME*, 1962, vol. 224, pp. 1047-61.
32. D. Kuhlmann-Wilsdorf: *Workhardening*, J. P. Hirth and T. Weertman, eds., pp. 97-139, Gordon & Breach, NY, 1968.
33. D. Kuhlmann-Wilsdorf: *Met. Trans.*, 1970, vol. 1, pp. 3173-79.
34. D. Kuhlmann-Wilsdorf: *Proc. Symp. Work Hardening Tens. Fatigue, 1975*, A. W. Thompson, ed., pp. 1-44, AIME, NY, 1977.
35. G. Langford and M. Cohen: *Trans. ASM*, 1969, vol. 62, p. 623.
36. J. D. Boyd, J. D. Embury, and C. M. Sargent: *Scr. Met.*, 1976, vol. 10, no. 10, pp. 901-03.
37. W. J. Witcomb: *Phys. Status Solidi*, 1974, vol. 22, pp. 299-304.
38. I. E. French and P. F. Weinrich: *Met. Trans. A*, 1976, vol. 7A, pp. 1841-45.
39. S. S. Hecker, L. E. Cox, and D. F. Stein: *J. Metals*, 1976, vol. 28, no. 12, p. A52.
40. L. E. Murr: *Interfacial Phenomena in Metals and Alloys*, p. 193, Addison-Wesley, Reading, MA, 1975.
41. T. Kovacs: *Met. Trans.*, 1971, vol. 2, pp. 961-66.
42. C. Zener: *Fracture of Metals*, p. 3, ASM, Cleveland, OH, 1948.
43. A. N. Stroh: *Phil. Mag.*, 1958, vol. 3, pp. 597-606.
44. W. D. Biggs and P. L. Pratt: *Acta Met.*, 1960, vol. 6, pp. 694-703.
45. D. Hull: *Acta Met.*, 1960, vol. 8, pp. 11-18.
46. R. Honda: *J. Phys. Soc. Jpn*, 1961, vol. 16, pp. 1309-21.
47. R. W. Cahn: *J. Inst. Metals*, 1955, vol. 83, pp. 493-96.
48. A. H. Cottrell: *Trans. TMS-AIME*, 1958, vol. 212, pp. 192-202.
49. A. W. Sleeswyk: *Acta Met.*, 1962, vol. 10, pp. 803-812.
50. K. Kitajima: *Proc. 1st Int. Conf. Fracture*, T. Yokobori and M. Ichikawa, eds., vol. 2, p. 659, Soc. Strength and Fracture of Materials, Tokyo, Japan, 1966.
51. T. Sakaki and T. Nakamura: *J. Iron Steel Inst. Jpn*, 1973, vol. 59, p. 955.
52. E. Hornbogen: *Trans. TMS-AIME*, 1961, vol. 221, pp. 711-15.
53. N. P. Allen, B. E. Hopkins, and J. McLennan: *Proc. Roy. Soc.*, 1956, vol. A234, pp. 221-46.
54. G. F. Bolling and R. H. Richman: *Can. J. Phys.*, 1967, vol. 45, pp. 541-57.
55. R. N. Gardner and H. G. F. Wilsdorf: *Proc. 4th Int. Conf. on Fracture*, T. M. R. Taplin, ed., vol. II, pp. 349-56, University of Waterloo Press, Waterloo, Canada, 1977.
56. H. P. Klug and L. E. Alexander: *X-ray Diffraction Methods*, p. 709, John Wiley & Sons, New York, 1974.
57. R. W. Bauer, R. N. Gardner, R. L. Lyles, Jr., T. C. Pollock, and H. G. F. Wilsdorf: *Proc. U.S.-Japan HVEM Seminar*, pp. 102-05, Honolulu, HI, Nagoya University, Nagoya, Japan, 1976.
58. T. Imura: Dislocation Movie Shown at the U.S.-Japan HVEM Seminar, Honolulu, December 6-10, Department of Metallurgy, University of Nagoya, Japan, 1976.
59. H. Fujita: Personal communication to H. G. F. Wilsdorf, Department of Materials Science and Engineering, Osaka University, Yamadakami, Suita 565, 1976.

DISTRIBUTION LIST

Copy No.	
1 - 12	Defense Documentation Center Cameron Station Alexandria, Virginia 22314
13	Office of Naval Research Department of the Navy 800 N. Quincy Street Arlington, Virginia 22217 Attention: Code 471
14	Office of Naval Research Department of the Navy 800 N. Quincy Street Arlington, Virginia 22217 Attention: Code 102
15	Office of Naval Research Department of the Navy 800 N. Quincy Street Arlington, Virginia 22217 Attention: Code 470
16 - 58	Basic Distribution (see attached pages)
59 - 104	Supplementary Distribution (see attached pages)
105 - 106	H. G. F. Wilsdorf
107	K. R. Lawless
108	I. A. Fischer Office of Sponsored Programs
109 - 110	E. H. Pancake Clark Hall
111	RLES Files

0949:jt

BASIC DISTRIBUTION LIST

Copy No.	
16	Commanding Officer Office of Naval Research Branch Office 495 Summer Street Boston, Massachusetts 02210
17	Commanding Officer Office of Naval Research Branch Office 536 South Clark Street Chicago, Illinois 60605
18	Office of Naval Research San Francisco Area Office 760 Market Street, Room 447 San Francisco, California 94102 Attention: Dr. P. A. Miller
19	Naval Research Laboratory Washington, D. C. 20390 Attention: Code 6000
20	Naval Research Laboratory Washington, D. C. 20390 Attention: Code 6100
21	Naval Research Laboratory Washington, D. C. 20390 Attention: Code 6300
22	Naval Research Laboratory Washington, D. C. 20390 Attention: Code 6400
23	Naval Research Laboratory Washington, D. C. 20390 Attention: Code 2627
24	Naval Air Development Center Code 302 Warminster, Pennsylvania 18974 Attention: Mr. F. S. Williams

BASIC DISTRIBUTION LIST (Continued)

Copy No.	
25	Naval Air Propulsion Test Center Trenton, New Jersey 08628 Attention: Library
26	Naval Construction Batallion Civil Engineering Laboratory Port Hueneme, California 93043 Attention: Materials Division
27	Naval Electronics Laboratory Center San Diego, California 92152 Attention: Electron Materials Sciences Division
28	Naval Missile Center Materials Consultant Code 3312-1 Point Mugu, California 93041
29	Commanding Officer Naval Surface Weapons Center White Oak Laboratory Silver Spring, Maryland 20910 Attention: Library
30	David W. Taylor Naval Ship R&D Center Materials Department Annapolis, Maryland 21402
31	Naval Undersea Center San Diego, California 92132 Attention: Library
32	Naval Underwater System Center Newport, Rhode Island 02840 Attention: Library
33	Naval Weapons Center China Lake, California 93555 Attention: Library
34	Naval Postgraduate School Monterey, California 93940 Attention: Mechanical Engineering Department

BASIC DISTRIBUTION LIST (Continued)

Copy No.	
35	Naval Air Systems Command Washington, D. C. 20360 Attention: Code 52031
36	Naval Air Systems Command Washington, D. C. 20360 Attention: Code 52032
37	Naval Air Systems Command Washington, D. C. 20360 Attention: Code 320
38	Naval Sea System Command Washington, D. C. 20362 Attention: Code 035
39	Naval Facilities Engineering Command Alexandria, Virginia 22331 Attention: Code 03
40	Scientific Advisor Commandant of the Marine Corps Washington, D. C. 20380 Attention: Code AX
41	Naval Ship Engineering Center Department of the Navy CTR BG #2 3700 East-West Highway Prince Georges Plaza Hyattsville, Maryland 20782 Attention: Engineering Materials and Services Office Code 6101
42	Army Research Office Box CM, Duke Station Durham, North Carolina 27706 Attention: Metallurgy & Ceramics Division

BASIC DISTRIBUTION LIST (Continued)

Copy No.	
43	Army Materials and Mechanics Research Center Watertown, Massachusetts 02172 Attention: Res. Programs Office (AMXMR-P)
44	Air Force Office of Scientific Research Bldg. 410 Bolling Air Force Base Washington, D. C. 20332 Attention: Chemical Science Directorate
45	Air Force Office of Scientific Research Bldg. 410 Bolling Air Force Base Washington, D. C. 20332 Attention: Electronics and Solid State Sciences Directorate
46	Air Force Materials Lab (LA) Wright-Patterson AFB Dayton, Ohio 45433
47	NASA Headquarters Washington, D. C. 20546 Attention: Code RRM
48	NASA Lewis Research Center 21000 Brookpark Road Cleveland, Ohio 44135 Attention: Library
49	National Burea of Standards Washington, D. C. 20234 Attention: Metallurgy Division
50	National Bureau of Standards Washington, D. C. 20234 Attention: Inorganic Materials Division

BASIC DISTRIBUTION LIST (Continued)

Copy No.	
51	Defense Metals and Ceramics Information Center Battelle Memorial Institute 505 King Street Columbus, Ohio 43201
52	Director Ordnance Research Laboratory P.O. Box 30 State College, Pennsylvania 16801
53	Director Applied Physics Laboratory University of Washington 1013 Northeast Fortieth Street Seattle, Washington 98105
54	Metals and Ceramics Division Oak Ridge National Laboratory P.O. Box X Oak Ridge, Tennessee 37380
55	Los Alamos Scientific Laboratory P.O. Box 1663 Los Alamos, New Mexico 87544 Attention: Report Librarian
56	Argonne National Laboratory Metallurgy Division P.O. Box 229 Lemont, Illinois 60439
57	Brookhaven National Laboratory Technical Information Division Upton, Long Island New York 11973 Attention: Research Library
58	Library Building 50, Room 134 Lawrence Radiation Laboratory Berkeley, California

SUPPLEMENTARY DISTRIBUTION LIST

Copy No.

59 Professor G. S. Ansell
Rensselaer Polytechnic Institute
Department of Metallurgical Engineering
Troy, New York 12181

60 Professor Dieter G. Ast
Cornell University
Department of Materials Science and Engineering
College of Engineering, Bard Hall
Ithaca, New York 14853

61 Professor H. K. Birnbaum
University of Illinois
Department of Metallurgy
Urbana, IL 61801

62 Dr. E. M. Breinan
United Technologies
Research Center
East Hartford, CT 06108

63 Professor H. D. Brody
University of Pittsburgh
School of Engineering
Pittsburg, PA 15213

64 Dr. Arthur E. Clark
Naval Surface Weapons Center
Solid State Division
White Oak Laboratory
Silver Spring, MD 20910

65 Professor J. B. Cohen
Northwestern University
Department of Material Sciences

66 Professor M. Cohen
Massachusetts Institute of Technology
Department of Metallurgy
Cambridge, MA 02139

67 Dr. Ronald B. Diegle
505 King Avenue
Columbus, Ohio 43201

SUPPLEMENTARY DISTRIBUTION LIST (Continued)

Copy No.	
68	Mr. G. A. DiPietro Advanced Vacuum Systems 30 Faulkner Street Ayer, MA 01432
69	Professor Thomas W. Eagar Massachusetts Institute of Technology Department of Materials Science and Engineering Cambridge, MA 02139
70	Professor B. C. Giessen Northeastern University Department of Chemistry Boston, MA 02115
71	Dr. G. T. Hahn Battelle Memorial Institute Department of Metallurgy 505 King Avenue Columbus, OH 43201
72	Dr. David G. Howden Battelle Memorial Institute Columbus Laboratories 505 King Avenue Columbus, OH 43201
73	Professor C. E. Jackson Ohio State University Department of Welding Engineering 190 West 19th Avenue Columbus, OH 43210
74	Dr. Lyman A. Johnson General Electric Company P.O. Box 8 Schenectady, NY 12301
75	Dr. C. S. Kortovich TRW, Inc. 23555 Euclid Avenue Cleveland, Ohio 44117
76	Professor D. A. Koss Michigan Technological University College of Engineering Houghton, MI 49931

SUPPLEMENTARY DISTRIBUTION LIST (Continued)

Copy No.	
77	Professor E. Laughlin Carnegie-Mellon University Schenley Park Pittsburgh, PA 15213
78	Professor A. Lawley Drexel University Department of Metallurgical Engineering Philadelphia, PA 19104
79	Dr. John Mahoney Phrasor Technology 110 South Euclid Avenue Pasadena, CA 91101
80	Dr. H. Margolin Polytechnic Institute of New York 333 Jay Street Brooklyn, NY 11201
81	Professor K. Masabuchi Massachusetts Institute of Technology Department of Ocean Engineering Cambridge, MA 02139
82	Dr. H. I. McHenry National Bureau of Standards Institute for Basic Standards Boulder, CO 80302
83	Professor J. W. Morris, Jr. University of California College of Engineering Berkeley, CA 94720
84	Professor Ono University of California Materials Department Los Angeles, CA 90024
85	Dr. M. Pakstys General Dynamics Electric Boat Division Eastern Point Road Groton, CT 06340

SUPPLEMENTARY DISTRIBUTION LIST (Continued)

Copy No.

86 Dr. Neil E. Paton
Rockwell International Science Center
1049 Camino Dos Rios
P.O. Box 1085
Thousand Oaks, CA 91360

87 Professor R. M. Pelloux
Massachusetts Institute of Technology
Department of Materials Science and Engineering
Cambridge, MA 02139

88 Mr. A. Pollack
David W. Taylor Naval Ship Research and
Development Center
Annapolis Laboratory
Annapolis, MD 21402

89 Dr. Karl M. Prewo
United Technologies Laboratories
United Technologies Corporation
East Hartford, CT 06108

90 Professor David Roylance
Massachusetts Institute of Technology
77 Massachusetts Avenue
Cambridge, MA 02139

91 Professor W. F. Savage
Rensselaer Polytechnic Institute
School of Engineering
Troy, NY 12181

92 Dr. C. Shaw
Rockwell International Science Center
1049 Camino Dos Rios
P.O. Box 1085
Thousand Oaks, CA 91360

93 Professor O. D. Sherby
Stanford University
Materials Sciences Division
Stanford, CA 94300

SUPPLEMENTARY DISTRIBUTION LIST (Continued)

Copy No.

94 Dr. R. P. Simpson
Westinghouse Electric Corporation
Research and Development Center
Pittsburgh, PA 15235

95 DR. W. A. Spitzig
U.S. Steel Corporation
Research Laboratory
Monroeville, PA 15146

96 Dr. E. A. Starke, Jr.
Georgie Institute of Technology
School of Chemical Engineering
Atlanta, GA 30332

97 Professor N. S. Stoloff
Rensselaer Polytechnic Institute
School of Engineering
Troy, NY 12181

98 Dr. E. R. Thompson
United Technologies Research Center
United Technologies Corporation
East Hartford, CT 06108

99 Professor David Turnbull
Harvard University
Division of Engineering and Applied Physics
Cambridge, MA 02139

100 Professor W. E. Wallace
University of Pittsburgh
Pittsburgh, PA 15260

101 Dr. F. E. Wawner
University of Virginia
School of Engineering and Applied Science
Charlottesville, VA 22901

102 Dr. C. R. Whitsett
McDonnell Douglas Research
McDonnell Douglas Corporation
St. Louis, MO 63166

SUPPLEMENTARY DISTRIBUTION LIST (Continued)

Copy No.

103 Dr. J. C. Williams
Carnegie-Mellon University
Department of Metallurgy and Materials Sciences
Schenley Park
Pittsburgh, PA 15213

104 Dr. M. A. Wright
University of Tennessee
Space Institute
Tullahoma, TN 37388